White Paper

Evaluating clinical performance of the new Coronis Fusion 6MP DL display

What's inside?

- Clinical performance of Coronis Fusion 6MP DL for lung nodule screening
- ROC curves for Coronis Fusion 6MP DL
- A framework for accurately determining clinical performance of a medical display

Cédric Marchessoux
Research engineer, PhD

Tom Kimpe
CTO MID

Barco Medical Imaging Division
Technology & Innovation Group

cedric.marchessoux@barco.com
tom.kimpe@barco.com

INTRODUCTION

Color displays are being used more and more in medical imaging. Obviously there are many advantages of using color displays. They are much more versatile than grayscale displays: they can be used to look at fused (multi-modality) images, 3D rendering looks much better and it is possible to show annotations in color for example when using CAD.

But an important concern so far has been whether color displays really can offer the same diagnostic quality as grayscale displays. To date color displays have had lower specifications of contrast and luminance when compared to monochrome displays.

This whitepaper describes the clinical performance of three display systems for lung nodule screening. The first display is a 3 MegaPixel standard color display, the second display is a medical Barco Coronis 3MP grayscale and the third display is the new color Coronis Fusion 6MP DL. The Coronis Fusion 6MP DL has a resolution of 6 MegaPixel and a size of 30.4” and as such can replace two 3 MegaPixel medical 20.8” color or grayscale displays.

TABLE OF CONTENTS

TABLE OF FIGURES

1 DISPLAY COMPARISON STUDY INTRODUCTION

Within Barco's Medical Imaging Division, a virtual image chain for perceived and clinical quality of medical displays has been developed (Medical Virtual Image Chain: MEVIC). This image chain is inspired by the Image Quality Circle developed by *Engeldrum* [Eng 00, Jun 01]. The circle is represented in figure 1. The image quality circle shows the different phases for controlling and simulating a complete chain in the domain of vision. The circle shows the links and relations between technology variables are controlled from a product to the physical image parameters obtained from system modelling. Too many engineers and researchers cease their efforts at this stage. In other words, they characterize a system by mean of physical parameters that they can measure and control. They are simply forgetting that they are developing applications with a final observer. The resulting image quality should be optimized and correlated to the human perception or customer perceived preferences. From technology variables to customer's preferences, the circle covers the complete chain. Thanks to the Image Quality Circle, a simulation platform can find correlations between perceived judgments and physical parameters by applying visual algorithms. The aim of MEVIC is to have a complete chain from the image capture part to the visualization in the context of medical displays. This paper presents a direct application of the MEVIC project and of the image quality circle; comparing and validating different medical displays.

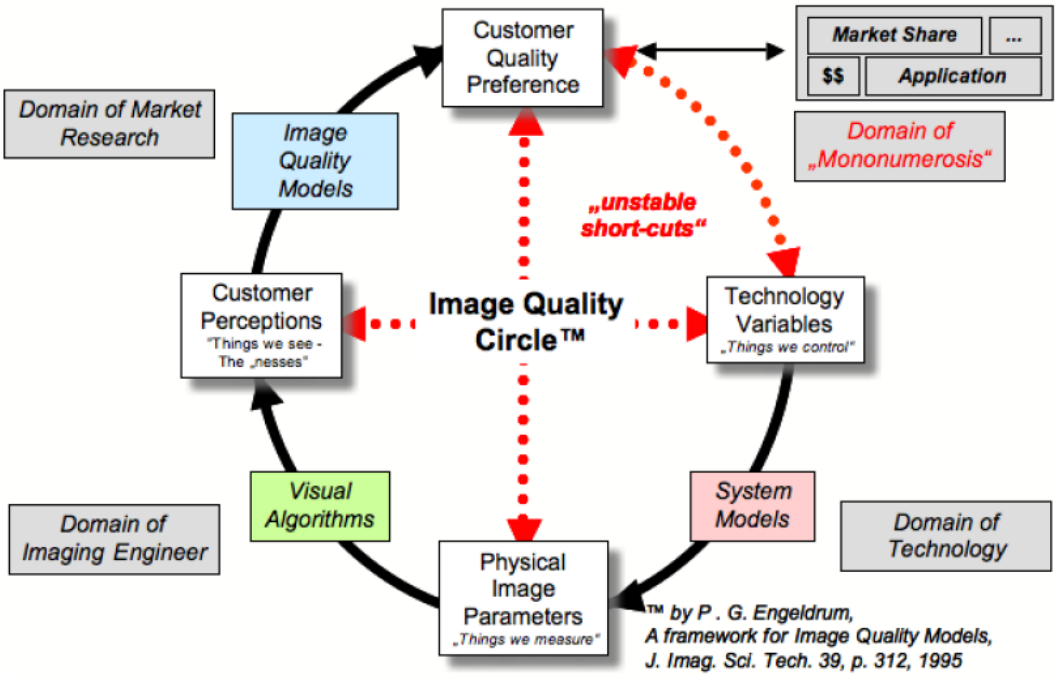

Fig. 1: the image quality circle

The aim of the study presented in this white paper is to develop and validate a new methodology for comparing medical displays by means of a clinically perceived image quality approach. Color displays are increasingly being used in medical imaging both for screening and primary diagnosis. The medical community is questioning whether medical color displays have sufficient clinical performance compared to medical grayscale displays and even whether consumer color displays can be used. This paper will give an answer by comparing the clinical performance for lung nodule detection by means of a numerical observer. We want to compare three LCD based displays: one medical grayscale display, a new medical color display (Coronis Fusion 6MP DL) and a standard color display. The new medical color display has higher luminance and lower spatial noise than the standard color display. The medical grayscale display delivers more luminance but has less spatial noise [Kim 05] compared to the new medical color display. Sets of healthy and diseased lung images will be used and in the healthy images simulated lesions with different controlled characteristics (size and density) are inserted.

In the context of MEVIC, two different Human Visual Observer Models (HVOM) have been developed. The first one is inspired by the JNDmetrix from Sarnoff institute (HVOM1) and the second one (HVOM2) is based on the Channelized Hotelling Model. HVOM1 allows obtaining map scores of perceivable differences (in terms of Just Noticeable Differences, JND) and HVOM2 can give the performance of the display evaluated. Figure 2 shows the different HVOMs in MEVIC. In this paper, the displays are not simulated. In other words: they are not virtual; images are shown on the display and then captured by an XYZ camera (see appendix A). This camera allows the acquisition of colored intensity maps in cd/m².

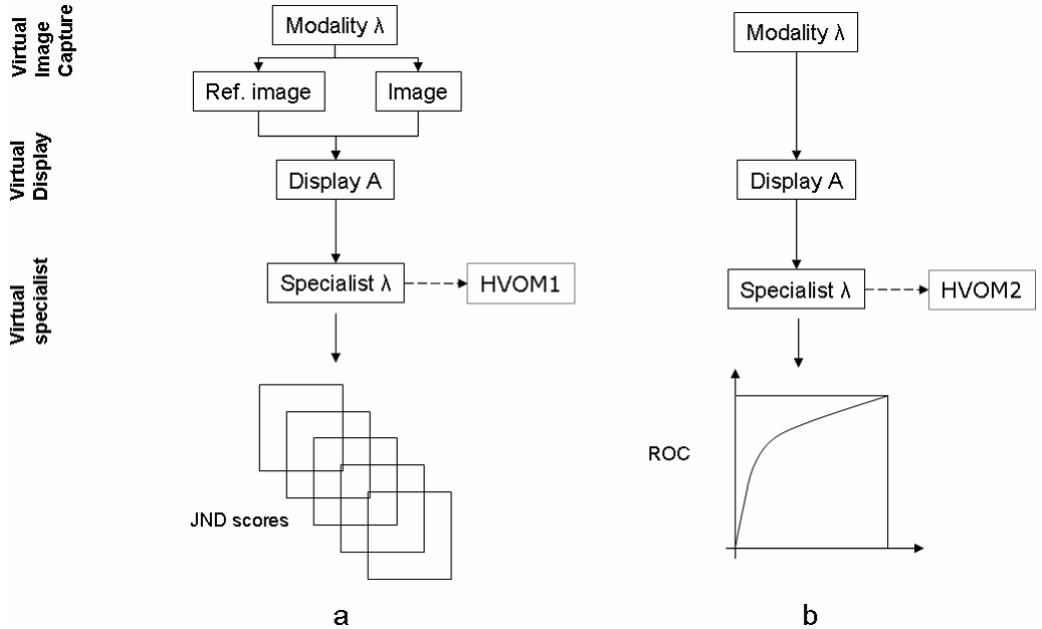

Fig.2: MEVIC platform for HVOM1 and HVOM2

The study will use three different monitors (see appendix B). Two of them are developed by Barco (Medical Imaging Division):

- BARCO Coronis 3MP grayscale display (20.8“)
- 3MP standard Color display (20.8“)
- BARCO Coronis Fusion 6MP DL display (30.4”)

To compare the 6MP display with the 3MP, the Coronis Fusion 6MP DL display is used in dual 3MP mode.

2 DISPLAY COMPARISON BASED ON HVOM1

2.1 Objective

To compare clinical performance of medical displays in terms of signal detection, a new methodology is presented as Human Visual Observer Model (HVOM1). The goal of the two HVOMs is the same: determine when the signal pathology) can be perceived on the displays, in order to estimate clinical display performance. For HVOM1, this will consist of the perceived contrast threshold, and for the HVOM2, it is based on a cancer detection task.

2.2 Description of HVOM1: JNDmetrix -IQ

For several years, multiple research groups have been modelling the various aspects of human perception to integrate them in a complete Human Visual System (HVS) and to develop visible image difference metrics. Some complete HVS models proposed in the literature such as the Visible Differences Predictor [Dal 93] or the Just Noticeable Metrix-IQ from the Sarnoff institute [Sar 07] result in visible differences maps, combining subjective and objective factors. In our framework we use JNDMetrix-IQ; a discontinued commercial product of Sarnoff Corporation, to compute JND values. This module, called "JNDModule" in the MEVIC platform, is the first Human Visual Observer Model (HVOM1) [Mar 08]. This JNDMetrix Human Visual System (HVS) is a reference in the medical domain [Lub 95]. It allows getting perceived differences map of two images displayed on a monitor. The image is decomposed per orientation and per band of spatial frequency. Edge enhancement, filtering, anisotropy, masking, color and temporal aspect effects are taken into account. The goal is to measure perceived differences between two images (a reference and a test image) or displays as global score, per frame and per channel. This is expressed using the Just Noticeable Difference (JND) metric. JNDs measure the degree to which the human eye can see distortions in an image or video sequence. Hence it reflects the human subjective assessment of images or video fidelity. JNDmetrix-IQ gives to each picture a JND score Φ. If the two pictures are exactly the same then they get a JND score $\Phi = 0$. If there are differences the frame gets a score different from 0, where $\Phi = 1$ agrees to the chance that an observer barely sees a difference between the two frames with a probability of 75%. This may seem a high probability, but one must take into account that the minimum is 50% due to the fact that if you show two pictures (A and B), and there is no visible difference, then 50% of a test audience will say A is better than B and vice versa. So a probability of 75% means that 75% of the test people will choose picture A above picture B, including the people that do not see the difference and guess. The designers of JND state that at a score $\Phi < 1$, there are no differences noticeable between the two pictures, even if one knows the exact place and nature of the difference in advance. At a score $\Phi = 3$, the differences are clearly visible when an observer knows the exact location in the picture. With a score $\Phi = 5$, the differences are clearly visible. For more

details, the reader can refer to the description of the implementation of HVOM1 [Mar 08]. The JND score will quantify the range of differences between the two images. The higher the score, the more visible the differences for the human eye will be. One possible representation is a color map where the perceived differences are mapped by means of a color Look Up Table (LUT), shown on figure 3. The JND scores are clipped to "5".

Fig. 3: look Up Table for HVOM1 (JND)

2.3 Dataset for HVOM1: X-ray chest images with nodules

For the HVOM1, i.e. JND, a reference image is used, coming from a real healthy X-ray image validated by a radiologist from the hospital of Ghent in Belgium. The image does not present any kind of abnormality. In this image, a signal (=lung nodule) is inserted of which the density is varied. The diameter of the signal is 30 pixels and does not change. The nodule insertion is done by using Samei's model [Sam 97]. Consequently, for this HVOM, the background always remains the same, only the signal density will change.

For HVOM1, a reference image and a test image are required to get JND differences (maps and JND scores). The reference image is an X-ray image of a healthy chest (cf. figure 4-a). Due to our measurement system, only a part of the image can be captured, therefore the original image is cropped to a resolution of 420 x 420 pixels (figure 3.7-b). This image is the reference image or background. To generate the signal present images (background + signal), artificial nodules are inserted. Lung nodules can be caused by lung cancer and need to be detected very early. Observer performance studies of subtle lung nodules are frequently used to evaluate new thoracic radiographic systems [Sam 03]. The use of simulated lung nodules has the advantage that the presence and location of the nodules are accurately known and the true-positive detection rates can be determined. The model used to simulate lung nodules was developed by Samei. The model was validated through clinical study [Sam 03] and has been accepted by the medical imaging community as realistic. The nodules were simulated to mimic the radiographic characteristics of tissue-equivalent lesions. The contrast of the simulated nodule is defined in terms of relative change in exposure-dependent linear detector signal ($\Delta E/E$). Furthermore, the simulated nodules have a circular symmetry and a contrast profile based on a mathematical function deduced from a database of real lung nodules [Sam 97]. The value of an image c at position $\vec{r}$ is given by:

$$c(\vec{r}) = C\left(\frac{4}{D^4}\left\|\vec{r}-\vec{r}_0\right\|^4 - \frac{4.2}{D^2}\left\|\vec{r}-\vec{r}_0\right\|^2 + 1\right) \text{ with } -0.6D \le \left\|\vec{r}-\vec{r}_0\right\| \le 0.6D \quad (1.1)$$

where c ($\vec{r}$) is the contrast profile as a function of radial distance r = $\|\vec{r} - \vec{r}_0\|$, C is the peak contrast value of the nodule, and D is the diameter of the nodule at the specified imaging plane. A typical value for the peak contrast-to-diameter ratio of a simulated nodule was 0.0098 mm^{-1}. The diameter chosen has a value of "30" pixels. The minimum contrast has a value of "0" and for the maximum, a value of "0.398". A complete set of images was generated with a step of 0.002 between 0 and 20% and equal to 0.008 for the end. The maximum density was normalized to "100" %. Further in this paper, the "density" term could be used as well as "contrast". An example of few images generated are shown on the figure 4-c.

The images are displayed on the 3 different monitors and captured by the XYZ camera (cf. Appendix A).

2.4 Expected results: HVOM1

Figure 5 corresponds to the curve that we expect to obtain for the different displays. This curve consists of two parts:

1. At low densities the signal is hidden by the constant noise level with JND values superior to "0". For color displays, this noise level is expected to be higher than for grayscale displays.
2. For higher densities, the signal should become higher than the noise and at the threshold value "1" JND at the viewing distance 45cm, the signal should become barely perceivable.

The first part of the curve represents the display noise. The point when the curve slope becomes important is the inflection point. This indicates the minimum perceivable contrast level for that display. The slope of the curve in the realm where the signal is higher than the noise is also important to note. Low contrast lesions can easily be masked by spatial noise present in the displays and there is a significant difference in spatial noise levels.

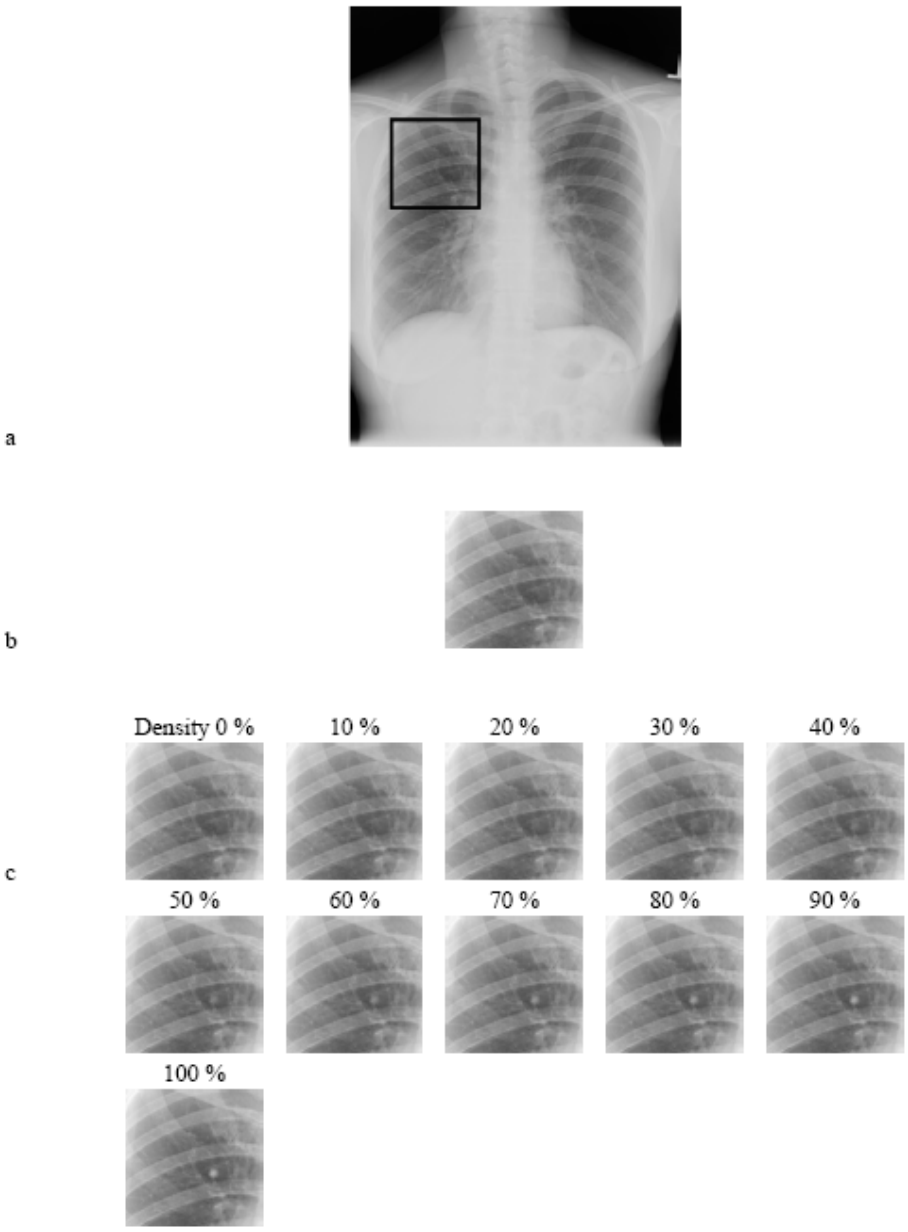

Fig. 4: a) original x-ray chest image (1536x2048 pixels) from JSRT [Shi 00] b) reference image: background, cropping of the original image (a) c) example of the background with signal inserted at different densities

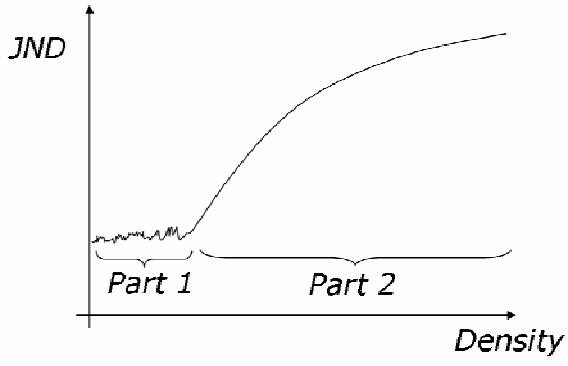

Fig. 5: expected results for HVOM1

2.5 Results

The results of figure 6 correspond to the expected results with a first part for low density signals corresponding to a preponderance of the noise and a second part where the signal is superior to the noise. At 45 cm viewing distance, at 1 JND the signal starts to be perceivable. The direct conclusion is: our new color Coronis Fusion 6MP DL display has the same performance as a 3MP grayscale display. Moreover, the clearly visible variations (oscillations) in the curve of the standard color display are coming from the fact that this display does not have backlight stabilization like the medical displays.

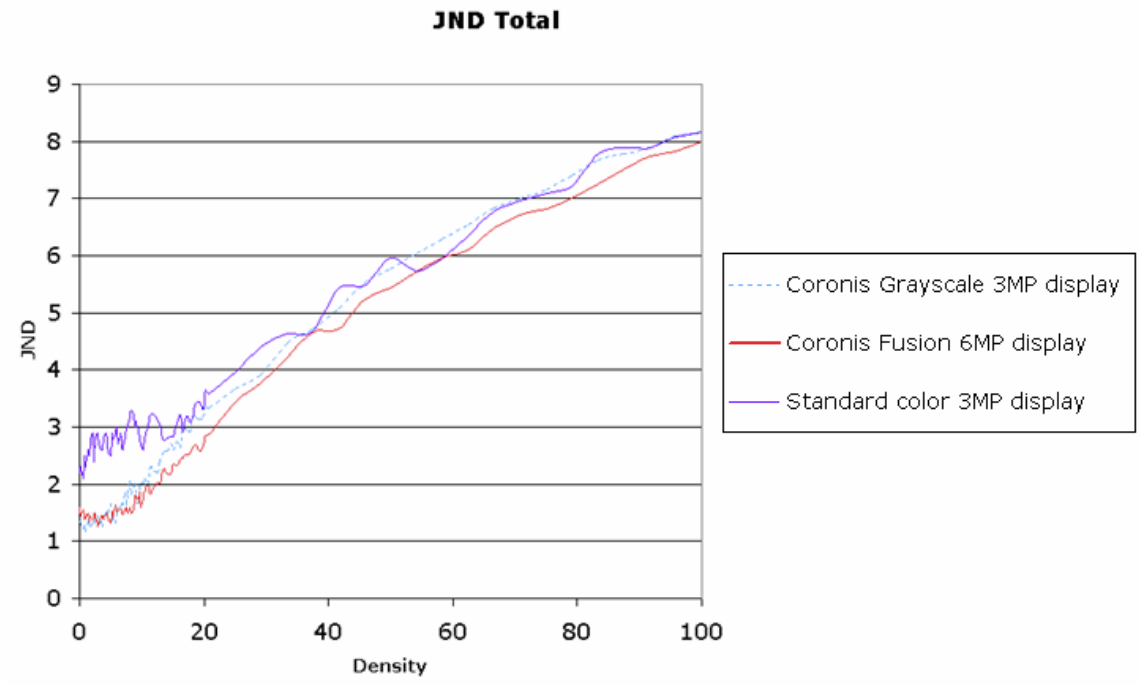

Fig. 6: JND vs. density results for the 3 different displays

3 DISPLAY COMPARISON BASED ON HVOM2: CHANNELIZED HOTELLING MODEL OBSERVER

3.1 Objective

In addition to the HVOM1 we implemented another HVOM based on the theory of signal detection for medical applications. The principle differs in comparison with HVOM1. We want to implement a numerical observer capable of distinguishing signals from background, where the signal to detect is an abnormality. The aim of this is to get ROC curves, allowing comparison of performance of different systems.

3.2 Description of HVOM2: Channelized Hotelling Model (CHM)

Ideal Bayesian observer
The discriminant function of the ideal observer [Bar 93] divides the conditional probability of the image given that the signal is present by the conditional probability of the image given that the signal is absent, i.e., $\lambda linear(g) = p(g|H_1)/p(g|H_0)$, where H_1 indicates the hypothesis, or condition, that the signal is present and H_0 indicates that the signal is absent. This function is known as the likelihood ratio [Bar 93]. The form of a linear computer observer for a binary lesion detection task is:

$$\lambda linear(g) = [g_1 - g_0]^t.K^{-1}.g \qquad (1.2)$$

where g_1 and g_0 are the means of the two classes of images with and without signals (abnormality), respectively [Bon 00]. The superscript t denotes a matrix transpose and K is a matrix that depends on the specific form of the observer. For a non-prewhitened observer it is simply the identity matrix, while for a prewhitened observer, K is a covariance matrix that decorrelates the noise in the images. Meaning that K^{-1} plays the role of a filter to reduce the noise in the image in order to facilitate the detection task. Indeed $[g_1 - g_0]$ corresponds to the signal. Multiplying the averaged signal $[g_1 - g_0]$ to an image g will result in a low score of $\lambda linear(g)$ if there is no signal in g and in high score if there is a signal.

Hotelling observer

$$W = [g_1 - g_0]^t.K^{-1} \qquad (1.3)$$

W is the template observer to apply on images for a detection task. The template observer should be first trained on a pre-known dataset where k (the covariance matrix) will be averaged for the different images of the training set.

Channelized hotelling observer
A special form of the equation 1.3 is the channelized hotelling observer in which the images g are filtered by frequency-selective channels that model

properties of the human visual system. This model has been shown to successfully reflect human performance in detecting hot lesions in nuclear medicine images under a wide range of conditions [Bon 00]. The model also successfully has been used to predict clinical performance of medical displays [Kru 04] and medical image processing algorithms [Eck 05]. The channels used are the Laguerre-Gauss functions (see figure 7) [Gal 03]. The main difficulty is the inversion of the covariance matrix. Moreover the choice of the number of channels needs special attention. Deciding on the number of channels can be done by means of a bibliographic study or by applying the CHM with different number of channels and selecting the minimum number of channels for which the performance is high. Two steps are required to run the CHM, first the observer template has to be trained and then to be tested. Therefore, two different datasets are necessary. The symmetrical (isotropic) signal (abnormality) should always be placed at the center of the image.

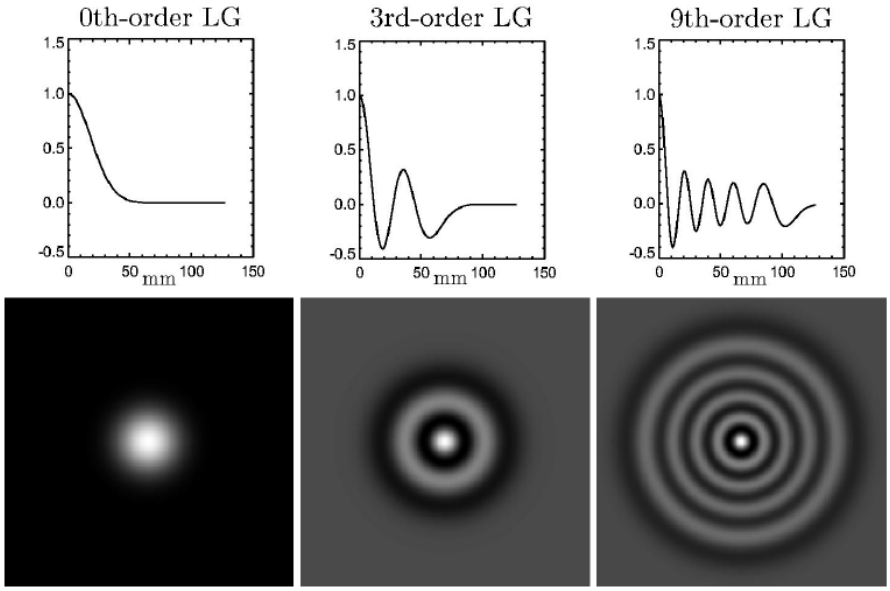

Fig. 7: example of Laguerre-Gauss functions [Gal 03]

Training phase

The training phase is done by giving a dataset of images for which the ground truth is known. This means that we need to know which images are healthy and which images are diseased and in that case where are the pathologies located. During the training phase the template W or the numerical observer is calculated. W has a size of MxM (with M=PxP, PxP: original image resolution).

Testing or simulation phase

The second phase of this program is the simulation phase. A new set of images is given to the trained observer, but in this case, the observer is tested on new images, healthy or diseased without giving knowledge on this dataset to the observer. Its goal is to classify these images as healthy or diseased. It will result in the following classification:

- True Positive: the observer correctly classifies the image as healthy.
- True Negative: the observer correctly classifies the image as diseased.
- False Negative: the observer wrongly classifies the image as diseased.
- False Positive: the observer wrongly classifies the image as healthy.

Following these results, a ROC with *Wilcoxon* AUC (Area Under the Curve) [Han 82] (Receiver Operating Curve) are calculated.

3.3 Expected results and interpretation: ROC curve

As explained before, the output of the simulation phase is the classification of each image of the dataset in four different groups: true positive, false positive, true negative and false negative. The aim is to generate a ROC curve, as presented in figure 8. This curve represents the sensitivity in function of (1 - specificity), in other words the true positive fraction in function of the false positive fraction.
An observer with very poor performance will have an AUC value close to 0.5. AUC value 0.5 means that the observer has the same performance as someone that is guessing (50% probability that the decision is correct). An observer with reasonable performance will have an AUC value superior to 0.8.

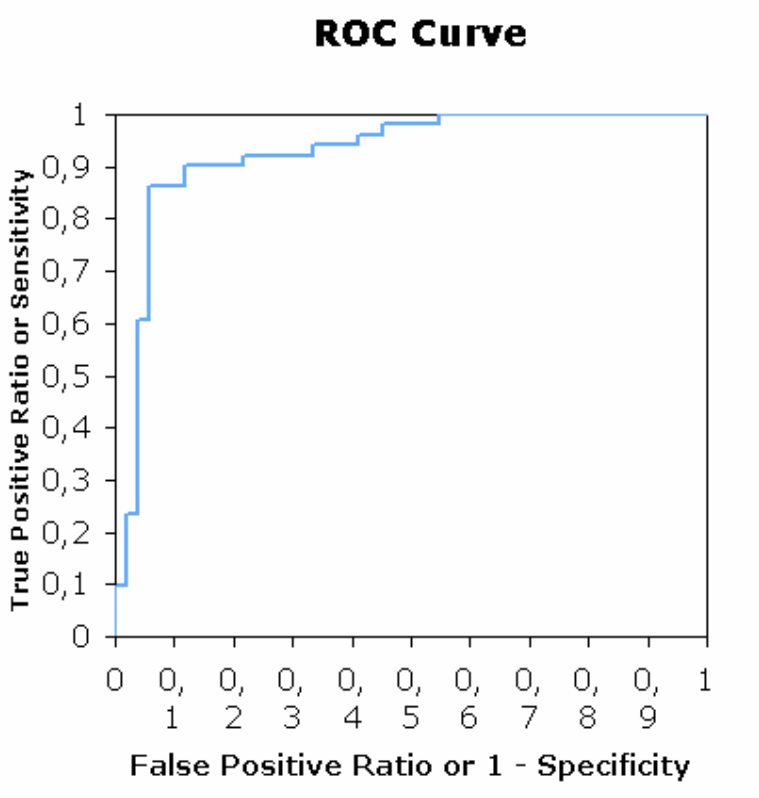

Fig. 8: example of ROC curve (Receiver Operating Curve)

3.4 Dataset for HVOM2: images

For the HVOM2, i.e. CHM, 380 images compose the dataset. These images are part of a Database from JSRT [Shi 00]. First they are cropped, and then a signal (still a nodule) is inserted in 190 images. The nodule density varies in a random process between the value 0.004948 and 0.05952 from Samei's model (cf. equation 1.1), corresponding to values between 1.2 and 3 JND from HVOM1. So this set of images is composed of 190 healthy images and 190 diseased images, grouped in two sub-sets, 190 images for the training phase and 190 images for the testing phase (cf. figure 9). The images are displayed on 3 different monitors and captured by the XYZ camera (see Appendix A).

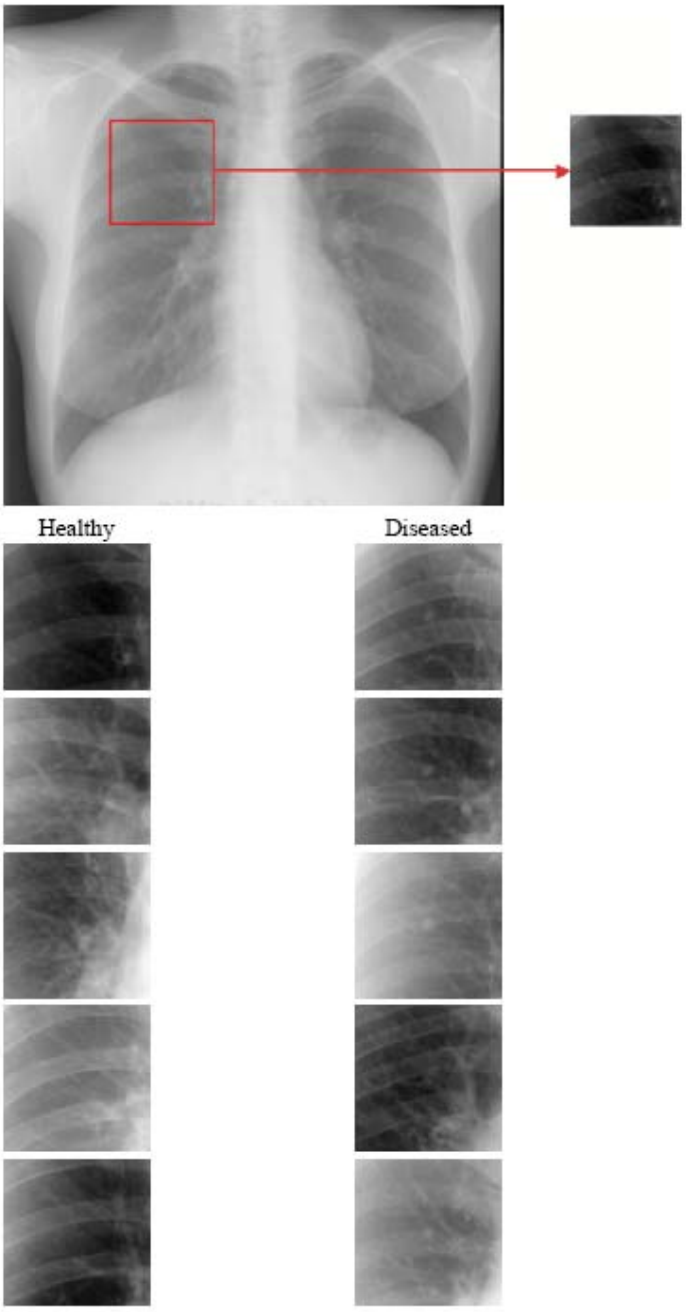

Fig. 9: examples of images from the dataset of images used for the Channelized Hotelling Model. Here, the density is 0.0035, and the diameter of the nodules is 30 pixels.

3.5 Results

Figure 10 and 11 represent the three ROC curves obtained for the three displays with the images captured by the XYZ camera. The AUC numbers are lower than usually found in the literature. This is due to the challenging images used for the study. Indeed, it would have been useless to study obvious cases with very easy positive cases. The contrast was chosen as a random number

for each background with a minimum and a maximum of 0.004948 and 0.05952 from Samei's model. In terms of JND, by looking to the figure 6, the contrasts correspond to values between 1.2 and 3 JND, meaning very challenging contrast nodule values to detect.

The AUC of the new Coronis Fusion 6MP DL display is equal to 0.79 +/- 0.023 and very close to the AUC from the medical gray display (AUC=0.80 +/ 0.023) even though there is a luminance difference of 100 cd/m² ($L_{max\_Coronis}$=500 cd/m² and $L_{max\_Coronis\ Fusion\ 6MP}$=400 cd/m²). It means than the performances of the new Coronis Fusion 6MP display could be even better with a luminance of 500 cd/m². The medical displays perform much better than the standard color display (AUC= 0.68 +/- 0.027). The reason why the AUC values are rather low (0.68 - 0.80) is because the clinical images that we used for this study are difficult cases. Many images contain very subtle lung nodules that are hard to detect. The standard color display that has been evaluated is a recent display with typical consumer specifications that are shown in appendix B. The fact that this display is performing much worse than the other medical displays can be explained by the absence of several technologies that are present in medical displays. The medical displays have a built-in light sensor to continuously stabilize the output of the display and to compensate for ambient light. In addition both medical displays also have technology to improve uniformity and reduce spatial noise ("Uniform Luminance Technology").

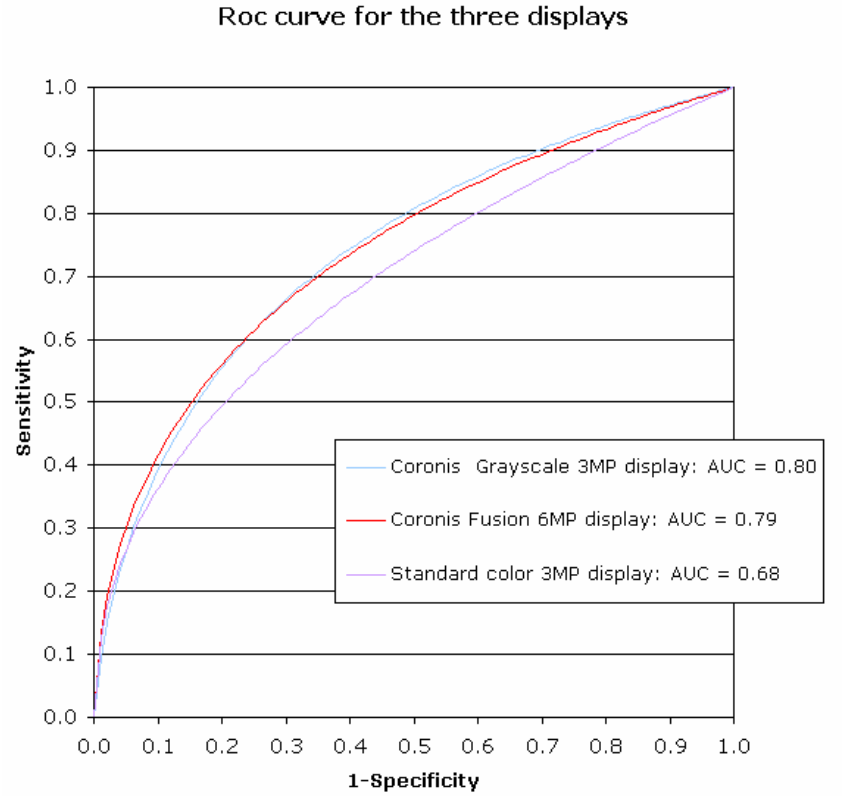

Fig. 10: ROC curve for the 3 displays with the images captured by the XYZ camera

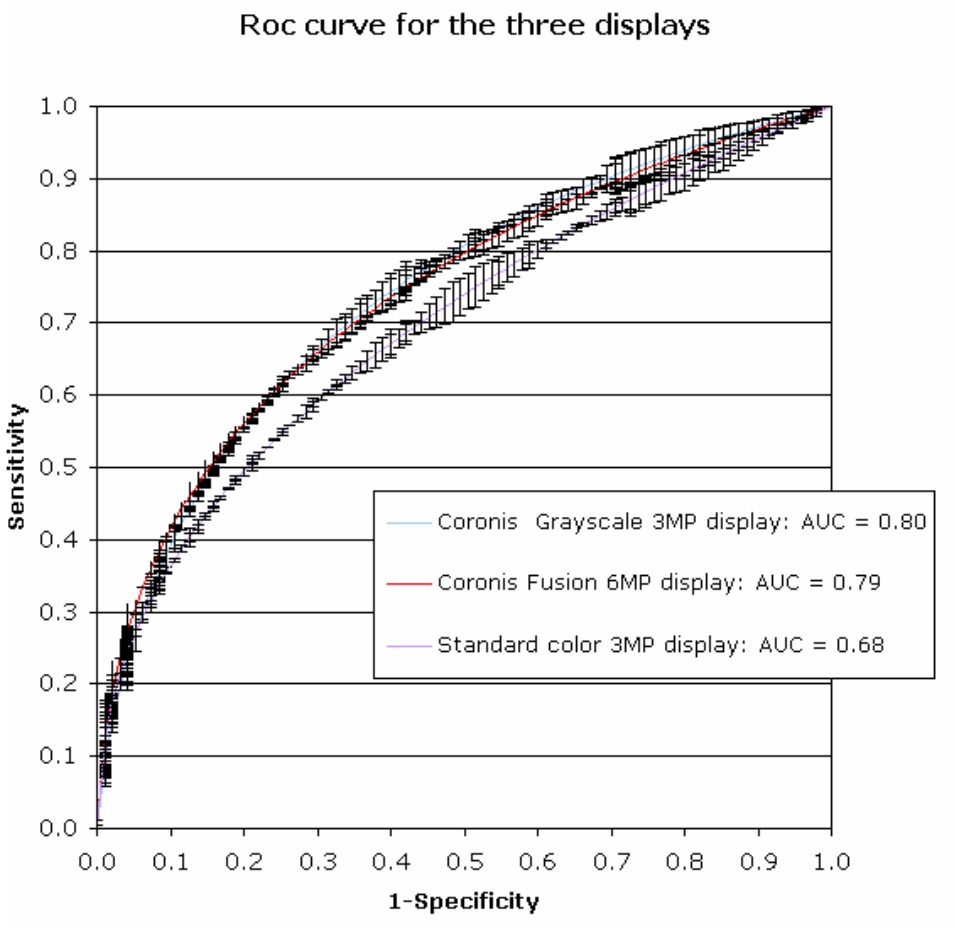

Fig. 11: ROC curve for the 3 displays with errors bars

CONCLUSIONS

In this whitepaper we compared the clinical performance of three displays for lung nodule screening: a standard 3 megapixel color display, a medical Barco Coronis 3MP grayscale and the new Coronis Fusion 6MP DL.

Two different methods were used to measure clinical performance of these displays. A first approach is based on the JNDMetrix platform that has been used many times to quantify performance of medical displays. The second approach uses the channelized hotelling model that is considered to be a standard for computing clinical performance of medical image processing and visualization systems.

This study was not performed as is often found in the literature - on a limited dataset of obvious lesions, but rather on a large lesion dataset where the lesion is very challenging to detect.

Both models show that the medical grayscale display and the Coronis Fusion 6MP DL display have the same clinical performance for lung nodule screening. Moreover, both displays perform much better than a standard color display.

This means that radiologists now can benefit from the color functionality of the Coronis Fusion 6MP DL without any decrease in clinical performance compared to a medical grayscale display.

4 REFERENCES

[Bar 93] BARRETT H.H., YAO J., ROLLAND J., and MYERS K.J. Model observers for assessment of image quality. Proc. Natl. Acad. Sci. USA, Vol. 90, pp. 9758-9765, November 1993

[Bon 00] BONETTO P., JINYI Q.I. and LEAHY R.M. Covariance approximation for fast and accurate computation of channelized hotelling observer statistics. *Nuclear Science Symposium, IEEE*, vol. 3, pp. 1383–1387, 2000.

[Dal 93] DALY S. The visible differences predictor: an algorithm for the assessment of image fidelity. *Digital images and human vision, MIT Press, Cambridge*, 1993. 179-205.

[Eng 00] P-G. Engeldrum. Psychometric scaling: a toolkit for imaging systems development. ISBN 0-9678706-0-7. Imcotek press, Winchester, USA, 2000.

[Eck 05] ZHANG Y., PHAM B. and ECKSTEIN M., Task-based model/human observer evaluation of SPIHT wavelet compression with human visual system-based quantization, Academic Radiology, Volume 12, Issue 3, Pages 324-336, 2005.

[Gal 03] GALLAS B.D. and BARRETT H.H. Validating the use of channels to estimate the ideal linear observer. *Journal of Opt. Soc. Am. A*, vol. 20, n_9, pp. 1725–1738, 2003.

[Kim 05] KIMPE T., XTHONA A., MATTHIJS P. and DE PAEPE L. Solution for Nonuniformities and Spatial Noise in Medical LCD Displays by Using Pixel-Based Correction, Journal of Digital Imaging, Springer New York, July 2005, vol. 18, no. 3, pp. 209-218

[Kim 07] KIMPE T., MARCHESSOUX C. and SPALLA G. Evaluating clinical performance of color and grayscale medical displays by mean of a numerical observer. *93rd Scientific Assembly and Annual Meeting of the Radiological Society of North America*, Chicago, November 2007. RSNA.

[Kru 04] KRUPINSKI E., JOHNSON J., ROEHRIG H., NAFZIGER J., FAN J. and LUBIN J. Use of a Human Visual System Model to Predict Observer Performance with CRT vs LCD Display of Images. Journal of Digital Imaging, Volume 17, Number 4 / December, 2004

[Jun 01] JUNG J., GEELEN R. and VANDENBROUCKE D. The virtual image chain: a powerful tool for the evaluation of the perceived image quality as a function of imaging system parameters. In *IS&T/PICS Conference Proceedings*, pages pp. 128–131, 2001.

[Lub 95] LUBIN J. A visual discrimination mode for image system design and evaluation, in Visual Models for Target Detection and Recognition, E. Peli, Ed. Singapore: World Scientific, 1995, pp. 207–220.

[Mar 08] MARCHESSOUX C., ROMBAUT A., KIMPE T., VERMEULEN B. and DEMEESTER P. Extension of a human visual system for display simulation. SPIE EI, 2008.

[Sam 97] SAMEI E., FLYNN M. J. and EYLER W. R. Simulation of subtle lung nodules in projection chest radiography. *Radiology*, vol. 202, n_1, pp. 117–124, Jan 1997.

[Sam 03] SAMEI EHSAN, FLYNN MICHAEL J, PETERSON EDWARD and EYLER WILLIAM R. Subtle lung nodules: influence of local anatomic variations on detection. *Radiology*, vol. 228, n_1, pp. 76–84, Jul 2003.

[Sar 07] http://www.sarnoff.com/research-and-development/vision-technologies

[Shi 00] SHIRAISHI J. and AL. Database for chest radiographs with and without a lung nodule: Receiver operating characteristic analysis of radiologists detection of pulmonary nodules. *AJR*, vol. 174, January 2000.

[Han 82] HANLEY J.A. and MCNEIL B.J. The meaning and use of the area under a receiver operating characteristic (ROC) curve. Radiology, 1982.

APPENDIX A

Measurement system

This camera is a Prometric, and allows taking pictures in the XYZ color space. This color space has been developed by the CIE (*Commission Internationale de l'éclairage*). The XYZ color space is illustrated with the figures 3.14 and 3.15. Finally, the pictures displayed on the different monitors are captured.

In the XYZ color space, the Y represents the luminance in cd/m². The images captured by the camera are not expressed directly in XYZ but in Yxy, another representation of XYZ with some normalization. Before working with the different files, the values need to be converted in XYZ.

APPENDIX B

Display characteristics:

Coronis 3MP grayscale display (Barco)

Technology: TFT AM LCD Dual Domain IPS technology
Active screen diagonal: 528 mm (20.8")
Active screen width: 424 mm (16.7")
Active screen height: 318 mm (12.5")
Pixel pitch: 0.207 mm (0.00815")
Resolution: 2048x1536 / 1536x2048
DICOM calibrated luminance (native white): 500 cd/m² (145.93 fL)
Contrast ratio: 900:1 (typ)
Viewing angle: 170°
Look up table: 12 bit
Image stabilization embedded I-Guard: YES
Uniform Luminance Technology: YES
Uniform Luminance Technology: YES
Ambient Light Compensation (ALC): YES
Rise time (black to white) 10% to 90% (typ/max): 25 ms

Coronis Fusion 6MP display (Barco)

Technology: TFT AM LCD IPS-PRO technology
Active screen diagonal: 771.441 mm (30.4")
Active screen width: 654.360 mm
Active screen height: 408.576 mm
Pixel pitch 0.1995 mm
Resolution: 3280x2048
DICOM calibrated luminance (native white): 400 cd/m²
Contrast ratio: 750:1 (typ)
Viewing angle: 178°
Look up table: 12 bit
Image stabilization embedded I-Guard: YES
Uniform Luminance Technology: YES
Ambient Light Compensation (ALC): YES
Cooling system adaptive fan control: YES
Rise time (black to white) 10% to 90% (typ/max): 9 ms

Standard color 3MP display

Technology: TFT AM LCD
Active screen diagonal: 20.8 inch"
Pixel pitch: 0.207 mm
Resolution: 2048 x 1536, 24-bit (16.7M Colors)
DICOM calibrated luminance: 200 cd/m²
Contrast ratio: 300:1
Rise time (black to white) 10% to 90% (typ/max): 50 ms